Developing wide-field spatio-spectral interferometry for far-infrared space applications

David Leisawitz *[a], Matthew R. Bolcar [a], Richard G. Lyon [a], Stephen F. Maher [a,b], Nargess Memarsadeghi [a], Stephen A. Rinehart [a], and Evan J. Sinukoff [a,c]
[a] NASA Goddard Space Flight Center, 8800 Greenbelt Rd., Greenbelt, MD, USA 20771-2400;
[b] Science Systems and Applications, Inc.; [c] Universities Space Research Association

ABSTRACT

Interferometry is an affordable way to bring the benefits of high resolution to space far-IR astrophysics. We summarize an ongoing effort to develop and learn the practical limitations of an interferometric technique that will enable the acquisition of high-resolution far-IR integral field spectroscopic data with a single instrument in a future space-based interferometer. This technique was central to the Space Infrared Interferometric Telescope (SPIRIT) and Submillimeter Probe of the Evolution of Cosmic Structure (SPECS) space mission design concepts, and it will first be used on the Balloon Experimental Twin Telescope for Infrared Interferometry (BETTII). Our experimental approach combines data from a laboratory optical interferometer (the Wide-field Imaging Interferometry Testbed, WIIT), computational optical system modeling, and spatio-spectral synthesis algorithm development. We summarize recent experimental results and future plans.

Keywords: Interferometry, spatio-spectral interferometry, double Fourier interferometry, imaging interferometry, wide-field imaging interferometry, far-infrared, SPIRIT, SPECS,

1. INTRODUCTION

Sensitive, high-resolution imaging and spectroscopy in the far-infrared are critical capabilities for future space missions designed to probe young stellar objects to learn how planets form and some become habitable; to find and characterize planets in protoplanetary and dusty debris disks; and to probe the sky deeply to learn how present-day galaxies developed from progenitor structures and early generations of star formation. These are the main scientific objectives of the Space Infrared Interferometric Telescope (SPIRIT),[1,2] the Far-Infrared Interferometer (FIRI),[3a] and the Submillimeter Probe of the Evolution of Cosmic Structure (SPECS),[4] all of which may rely on wide-field spatio-spectral optical interferometry for their high-resolution imaging and spectroscopic capabilities.

With the possible exception of detector technology, the greatest challenge for far-IR interferometry is to demonstrate that the interferometer will actually produce the images and spectra necessary to satisfy mission science requirements. This is our objective. Over the past decade we have gained experience with wide-field spatio-spectral interferometry, and have made progress in understanding the technique's practical limitations. This measurement approach remains viable for future space applications in the far-infrared. In the near term, the technique will be applied on NASA's Balloon Experimental Twin Telescope for Infrared Interferometry (BETTII).[5,6]

This paper is the latest in a series,[7-17] to report on progress and plans in our effort to develop wide-field spatio-spectral interferometry. In Section 2, we summarize the case for wide-field spatio-spectral interferometry. Our experimental approach is described in Section 3. Recent accomplishments and future plans are summarized in Sections 4 and 5, respectively. A few concluding remarks are given in Section 6.

Two companion papers in this proceedings volume describe the hyperspectral scene generator used in our experiments[18] and the algorithm we developed to synthesize spatial-spectral data cubes from laboratory-generated and synthetic spatio-spectral interferometric data sets.[19]

* David.T.Leisawitz@nasa.gov; phone 1 301 286-0807

2. THE CASE FOR WIDE-FIELD SPATIO-SPECTRAL INTERFEROMETRY

The *Herschel Space Observatory* provides unprecedented angular resolution in the far-IR (7 arcsec at 100 μm), but an additional order-of-magnitude gain is needed to resolve developing planetary systems and beat extragalactic source confusion at these wavelengths. To achieve this resolution gain, a single-aperture telescope would have to be 10 times larger than *Herschel*, or about 40 meters in diameter. Such a telescope would be prohibitively expensive and over-designed in terms of light-collecting capability to satisfy the science community's requirements. Quoting Harwit *et al.*: "As amply illustrated by the performance of the small FIR/SMM space telescopes already launched, the light gathering power of telescopes is now somewhat of a secondary concern, given the strong signals and high numbers of photons obtained from astronomical sources and the exquisite sensitivity of detectors developed to date."[4]

Interferometry is an affordable way to bring the benefits of high resolution to space far-IR astrophysics. The light collecting telescopes in the interferometer can be sized to satisfy sensitivity requirements. Around years 2004-05, NASA sponsored studies of two far-IR interferometers, SPIRIT and SPECS, as well as the Single Aperture Far-IR (SAFIR) telescope. The SPIRIT study yielded a design reference mission, a mature pre-Phase A design concept, and an independently validated grass roots cost estimate.[1,2] SPIRIT is considerably less expensive than a 10-m single aperture cryogenic far-IR telescope, and the interferometer would provide much better angular resolution. SPIRIT matches the sub-arcsecond resolution of the James Webb Space Telescope (JWST) at 10 times longer wavelengths.

Because wavefront sensing and control (WFS&C) grows easier with increasing wavelength, space-based far-IR interferometry is not as difficult as it may seem. The WFS&C system for JWST is flight-ready for this *near*-IR application, where it will be used periodically to align the 18 segments comprising a 6.5-m diameter primary mirror.[20] An interferometer is the optical analog of a pair of JWST mirror segments.

While spatial and spectral techniques have been used separately in optical interferometry for a century, the combined technique has not matured sufficiently for use in a NASA mission. Michelson and Morley famously employed a technique similar to Fourier transform spectroscopy, in which light from a source is split into two beams and recombined after a moving mirror inserts a variable optical delay between one beam and the other.[21] The combined light can be recorded on a single detector or camera pixel. The output signal intensity, when plotted against the optical delay, makes an *interferogram*. The spectrum of the source can be constructed from the Fourier transform of the interferogram. If the optical delay range $R\lambda$ is sampled, the resulting spectral resolution will be R ($=\lambda/\Delta\lambda$). Michelson and Pease used spatial interferometry to measure stellar diameters.[22] In imaging interferometry, spatial coherence ("fringe visibility")* measurements at many interferometric baselines (telescope spacings and orientations) are Fourier transformed to produce an image. Each baseline samples a spatial Fourier component of the brightness distribution of the target scene, a component commonly identified by its coordinates in the spatial frequency u-v plane. The Van Cittert-Zernike theorem[23] explains that an image can be constructed without information loss if enough u-v plane positions are sampled. Mariotti and Ridgway described the possibility of obtaining spatial and temporal coherence measurements with a single instrument to obtain both image and spectral information.[24]

With one further natural extension, which is the substitution of a detector array for a single-pixel detector, a spatio-spectral interferometer can provide a wide field-of-view (FOV), in addition to high spatial resolution and moderately high spectral resolution. A conventional imaging interferometer has a FOV dictated by the diffraction-limited response of the individual light collecting telescopes, $\theta_p \sim \lambda/D$, for telescope diameter D. Radio astronomers call this the *primary beam* and use *mosaicing* methods to image larger areas.[25, 26] Light from many field angles, including angles $\theta > \theta_p$, can be focused onto the multiple pixels in a detector array to capture the interference fringe patterns from a wide FOV, as illustrated in Figure 1. If the optical design sets the plate scale to sample the primary beam with a single pixel, for example, then the imaged field can be expanded to a diameter $\theta_{FOV} = N\theta_p$, where N is the pixel count along one row or column of the array. An interferometer constructed with 1-m telescopes operating at 30 μm would have a primary beam $\theta_p = 0.1$ arcmin (1/33rd the diameter of the Hubble Ultra Deep Field), however the FOV can be expanded to 1.7 arcmin with a 16 × 16 pixel detector array. Many of the astronomical targets of interest are larger than a typical primary beam but fit within a 1 or 2 arcmin FOV. Many other targets, such as the galaxies in a "deep field" or the forming planetary

---

* "Visibility" refers to the amplitude of the envelope of the interference fringe pattern and is approximately $V = (I_{max} - I_{min})/(I_{max} + I_{min})$, where I_{max} and I_{min} are the maximum (constructive interference) and minimum (destructive interference) intensities.

systems in a cluster of protostars, can be observed in parallel with a field this size. Without the enhanced FOV, an imaging interferometer could observe clustered objects in series, but the observing efficiency would be extremely low because a complete set of observations covering many baselines would be required for each object. A detector *array* enables *parallel* observations of the interference fringes from sources at field angles $\theta > \theta_p$ if the optical delay range $b\sin\theta_{\|}$ is covered to compensate path-length differences external to the instrument, where b is the telescope separation, or baseline length, and $\theta_{\|}$ is the component of θ parallel to the baseline. A spectral resolution requirement also drives the optical delay scan range. If $R = 1000$, $\lambda = 30$ μm, $b = 30$ m, and $\theta_{\|} = 1.7$ arcmin, for example, the optical delay scan would have to cover 3 cm for spectroscopy and 1.5 cm to cover the wide FOV. The fact that these numbers are comparable makes FOV enhancement an obvious choice. The additional scan time needed for the wide FOV is smaller than the time needed for spectral resolution, so there is a tremendous efficiency gain over serial observations of multiple small FOVs. Further, a single scan mechanism can provide the optical delay. The scan mechanism could be similar to those used successfully in the cryogenic COBE FIRAS spectrometer, or the cold *Cassini* CIRS instrument.

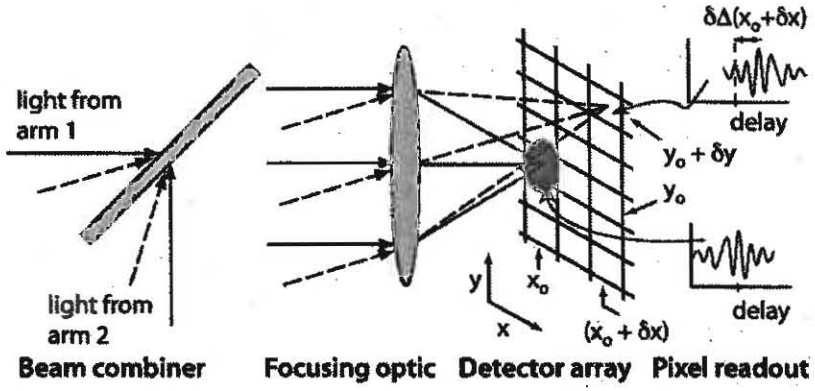

Figure 1. Interference fringes from field angles outside the primary beam (red ellipse) can be recorded simultaneously in the separate pixels of a detector array. If light from a source located on the optical axis of the interferometer (solid lines) is focused onto pixel (x_o, y_o), then light from an off-axis source (dashed lines) might reach pixel $(x_o+\delta x, y_o+\delta y)$ after traversing opposite arms of the interferometer. The white light fringe packet in the interferogram from the latter pixel (top) is displaced relative to the interferogram from the on-axis source (bottom). The detector array size (pixel count) determines the field-of-view.

3. EXPERIMENTAL APPROACH

To achieve the objective set out in Section 1, we take an approach similar to that used to verify performance of the JWST WFS&C system.[20] The key elements of our approach are as follows:

- Observe astronomically representative test scenes with an optical scale model (hardware testbed) equivalent in functionality and performance to a space far-IR interferometer.
- Compare observed interferograms with those predicted by a high-fidelity computer model of the testbed in which error terms associated with individual hardware components are modeled and can be switched on or off. Understand and document the effects of all significant error terms and sources of fringe visibility loss.
- Compare spatial-spectral data cubes derived from the interferometric data with "truth images" of the observed test scenes. Explain all significant differences between the derived output and the measured input images in terms of factors relevant to a far-IR interferometer in space, such as imperfect optical components and detectors, undersampling of the spatial Fourier components, photon noise, motion smearing, and artifacts associated with image construction.†
- Learn and document the practical limitations of wide-field spatio-spectral imaging interferometry when this technique is applied to astronomically relevant observations.

† Throughout this paper we use the term "image construction" or "synthesis" to refer to the computation of a three dimensional spatial-spectral data cube (a.k.a. hyperspectral image cube) from spatio-spectral interferometric data. This is analogous to conventional image synthesis, except that a third (spectral) dimension is included.

3.1 Hardware, facilities, and software

3.1.1 The Wide-field Imaging Interferometry Testbed (WIIT)

The Wide-field Imaging Interferometry Testbed[7] is a 1:150 functional scale model of the space far-IR interferometer SPIRIT. WIIT was designed to observe complex scenes representative of far-IR astronomical fields. It provides full u-v plane coverage and a wide FOV. WIIT operates at visible rather than far-IR wavelengths for several practical reasons: (a) the optical apertures and the delay line are scaled down from those intended for a far-IR instrument in proportion to the wavelength; (b) a CCD detector with sensitivity limited by photon noise (as expected in a cold far-IR space interferometer) was commercially available and affordable; (c) many other parts, such as translation and rotation stages, were available off-the-shelf and inexpensive; and (d) a commercial optical metrology system accurate to 10 nm was affordable.[9]

Figure 2 can be used to visualize the light path through WIIT. Light from a test scene located at the focus of a 21-inch diameter parabolic mirror is projected into the interferometer, mimicking a source in the sky. Two flat collector mirrors intercept separate portions of the incident wavefront, establishing an interferometric baseline. The separation between the collector mirrors can be adjusted to vary the baseline length, and the test scene can be rotated to vary the baseline orientation, enabling a full exploration of the u-v plane. The maximum baseline length is about 230 mm, so the achievable angular resolution $\theta_{res} = \lambda/2b_{max} = 0.27$ arcsec at $\lambda = 600$ nm. Two 25-mm diameter (D) collimated beams traverse the WIIT interferometer, starting at the collecting mirrors and reflecting off of flat mirrors until they merge orthogonally and combine at a half-reflective/half-transmissive parallel-plate beamsplitter. The primary beam width θp ($=1.2\lambda/D$) is 5.8 arcsec. Each WIIT CCD pixel subtends 1.6 arcsec.

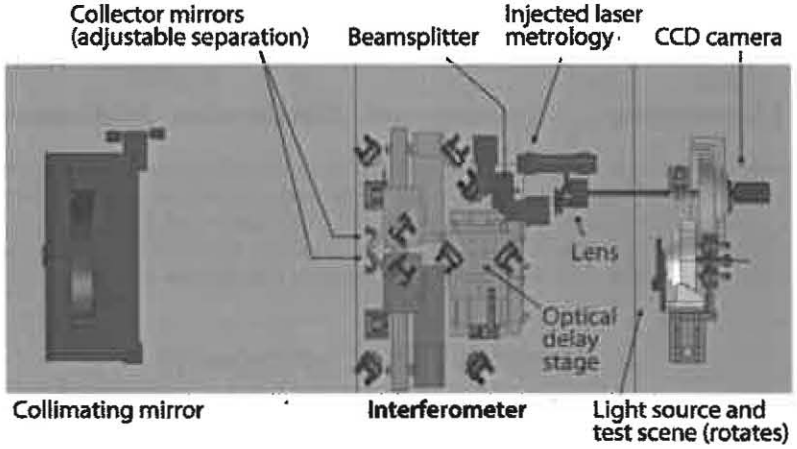

Figure 2. In this illustration, all of the major components of WIIT are shown to scale. The distance from the test scene to the collimating mirror is 2.43 m.

3.1.2 The Advanced Interferometry and Metrology (AIM) Lab

WIIT is housed in one of the two experiment bays of the Goddard AIM Lab. The AIM Lab is a world-class facility, which was developed with the requirements of this particular experiment in mind. A combination of thermal stability, acoustic isolation, passive and active vibration control, and gentle, laminar air flow in a clean room make this the ideal environment in which to collect data with WIIT. The data we obtain with WIIT in the AIM Lab are practically free of environmentally induced errors (i.e., wavefront distortion due to air turbulence, temperature and humidity fluctuations, and vibrations). In the AIM Lab, WIIT replicates the functionality and performance of a space interferometer: all significant error and noise sources are due to the instrument and quantifiable.

3.1.3 The Calibrated Hyperspectral Image Projector (CHIP)

As described in a companion paper,[18] CHIP serves as a flexible scene generator/light source for WIIT. It is installed at the location of the light source in Figure 2. The CHIP uses two Digital Light Processing (DLP) digital micromirror devices (DMDs) to create a customized, spectrally-diverse scene with good dynamic range. The CHIP is based on a prototype unit developed by the Optical Technologies Division at NIST.[27,28] One DMD is used with a prism and a

broadband light source to create a spectral engine, where the columns of the DMD are mapped to individual wavelengths. The shape of the output spectrum is determined by specifying the number of pixels to activate in each column. The second DMD creates the spatial scene, in much the same way as a commercial video projector. By synchronizing specific spectral basis functions with the corresponding spatial locations in the scene that contain those spectra, spatially-spectrally complex images can be generated and projected into WIIT. CHIP is capable of producing arbitrary spectra in the band between 380 nm and 780 nm with a spectral resolution of 5 nm. Thus, for example, CHIP can be used to project a galactic image in which the individual pixels are each assigned a spectrum with simulated continuum and spectral line emission. CHIP provides a hyperspectral scene to WIIT with spatial features as small as 0.13 arcsec, i.e., matched to the resolution limit of the interferometer. The CHIP scene is computer generated and synchronized with the WIIT CCD camera exposures and optical delay line motion. This synchronization also enables simulation of interferometer rotation and motion smearing associated with on-the-fly observing.

3.1.4 The Spatio-spectral Interferometer Computational Optical Model (SsICOM)

The Spatio-spectral Interferometer Computational Optical Model is a high-fidelity analytical model of WIIT. Output data files from SsICOM are identical to the Flexible Image Transport System (FITS) files that come from WIIT, but they contain simulated data. We use the non-sequential optical system modeling software FRED from Photon Engineering, LLC to develop SsICOM because FRED properly handles coherence properties of the traced rays. SsICOM includes Zernike polynomial parametric representations of the WIIT optical components based on lab measurements of the individual mirrors and beamsplitter,[9] and properly maps the light onto a focal plane with detector pixels matching those in the WIIT CCD camera.[12,14,17] SsICOM includes FRED scripts that: (a) simulate the scanning optical delay line, (b) sample a prescribed series of interferometric baselines, and (c) represent the input test scene. SsICOM treats the scene as a collection of point sources. It launches the desired number of light rays (with the desired wavelength distribution) from these point sources into the model interferometer, follows them as they traverse both arms of the interferometer and merge at the beamsplitter, images the pupil through a lens system matching the WIIT configuration, and calculates the intensity in each detector pixel as a function of delay line position, producing an interferometric data cube with two image dimensions (corresponding to WIIT pixels) and a third optical delay dimension (i.e., each pixel contains an interferogram). A software switch is used to activate or deactivate imperfections associated with each individual optical element, and artificial shot noise can be added to model photon-counting statistics. With all imperfections activated, SsICOM models WIIT; with all imperfections de-activated, SsICOM predicts the performance of an ideal wide-field spatio-spectral interferometer.

3.1.5 The Spatio-spectral Synthesis Software (S4)

Our Spatio-spectral Synthesis Software implements the algorithm described in a companion paper[19] and computationally processes the interferometric data cubes mentioned above to produce a single spatial-spectral cube with two high-resolution (θ_{res}; see Section 3.1.1) image dimensions and a third spectral dimension. The output spatial-spectral cube is an integral-field spectroscopic representation of the observed or modeled scene. Input to S4 comprises as many interferometric data cubes as desired, where each such cube corresponds to a unique interferometric baseline measurement (length and position angle). A WIIT observation of a single test scene typically yields several hundred interferometric data cubes, as the u-v plane is densely sampled. All or a subset of the data files can be fed into S4 to test the effect of undersampling spatial Fourier components and compare with analytical predictions.

3.2 Methodology

Our aim is to demonstrate the viability of spatio-spectral interferometry in realistic circumstances, recognizing that far-IR astronomical sources are spatially and spectrally complex. Since CHIP was integrated into WIIT, we have observed several simple test scenes, thus far repeating earlier measurements based on observations of scenes in which the spectrum was spatially invariant and multi-colored LEDs or a broad-band white light source were used for illumination. The response of the interferometer to a simple scene is easy to understand from a theoretical or intuitive point of view. CHIP will ultimately enable us to observe astronomically realistic scenes. Figure 3 illustrates our experimental approach.

SsICOM serves as a powerful diagnostic tool. We compare SsICOM-simulated and WIIT-observed interferograms to verify that the observed interferograms have the expected shapes and amplitudes, even when the scenes are spatially and spectrally complex. As shown in Section 4, we have already done this for simple scenes. Simulated data from SsICOM are fed into S4 to isolate the effects of synthesis processing on data quality. When the optical component imperfections are turned off and "noiseless" data are fed into S4, differences between the output spatial-spectral cube and the modeled scene can be ascribed to the synthesis algorithm if the u-v plane is densely sampled. Our aim is to determine the

contributions of individual error sources (e.g., imperfect optical components, photon noise) to discrepancies between the input "truth" and output "constructed" data cubes by activating a single error source at a time in SsICOM.

Finally, by learning how each critical design parameter affects the data quality, we will determine practical engineering steps that can be taken to build a wide-field spatio-spectral interferometer whose performance approaches fundamental limits.[29,30]

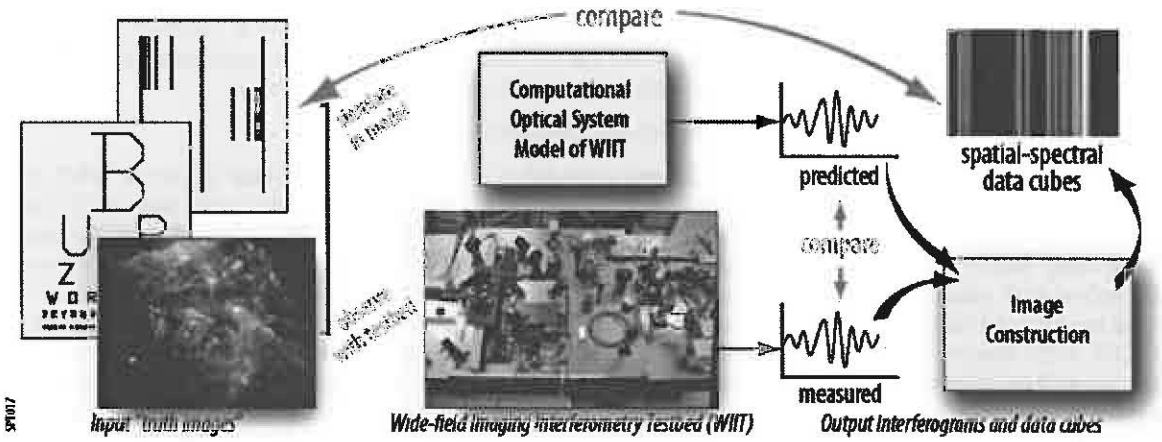

Figure 3. We apply an error-tracking experimental approach in which increasingly complex, more astronomically realistic test scenes are observed, and different observing modes are explored to learn the practical limitations of wide-field spatio-spectral interferometry and to quantitatively understand how each instrument design parameter impacts the quality of the synthesized hyperspectral image cube.

4. RECENT ACCOMPLISHMENTS

Since our initial report on progress and plans,[7,8,9] we have developed, refined, and tested all of the hardware and software elements described in Section 3.1, followed the experimental approach described in Section 3.2, and periodically reported on progress. WIIT was the first testbed to operate in the AIM Lab when this facility was completed in 2007, and it took a while to diagnose and shake out bugs in the Lab's air-handling system. Our perseverance was eventually rewarded with high-quality data.

During the past several years we have:

1. moved WIIT from its development lab to the AIM Lab and demonstrated the performance improvement expected when environmental conditions have a negligible effect on data quality;
2. used WIIT to observe a wide variety of simple test scenes;
3. verified the performance of a high-fidelity computational optical system model of the testbed, SsICOM, by comparing simulated interferometric data with theoretical predictions and measured data, as illustrated in Figure 4;
4. developed a better understanding of the visibility loss and error terms applicable to WIIT (Tables 1a and b, respectively, updated from Rinehart et al. (2004)[10] to include a new camera with 16-bit dynamic range and the improved environment of the AIM lab);
5. developed a spatio-spectral synthesis algorithm and implemented the algorithm in the S4 synthesis software, enabling construction of spatial-spectral data cubes from the inteferometric data (Figure 5); and
6. developed and integrated into WIIT a hyperspectral image projector, CHIP, to enable experimentation with astronomically realistic test scenes with details fine enough to test the resolution limit of WIIT.

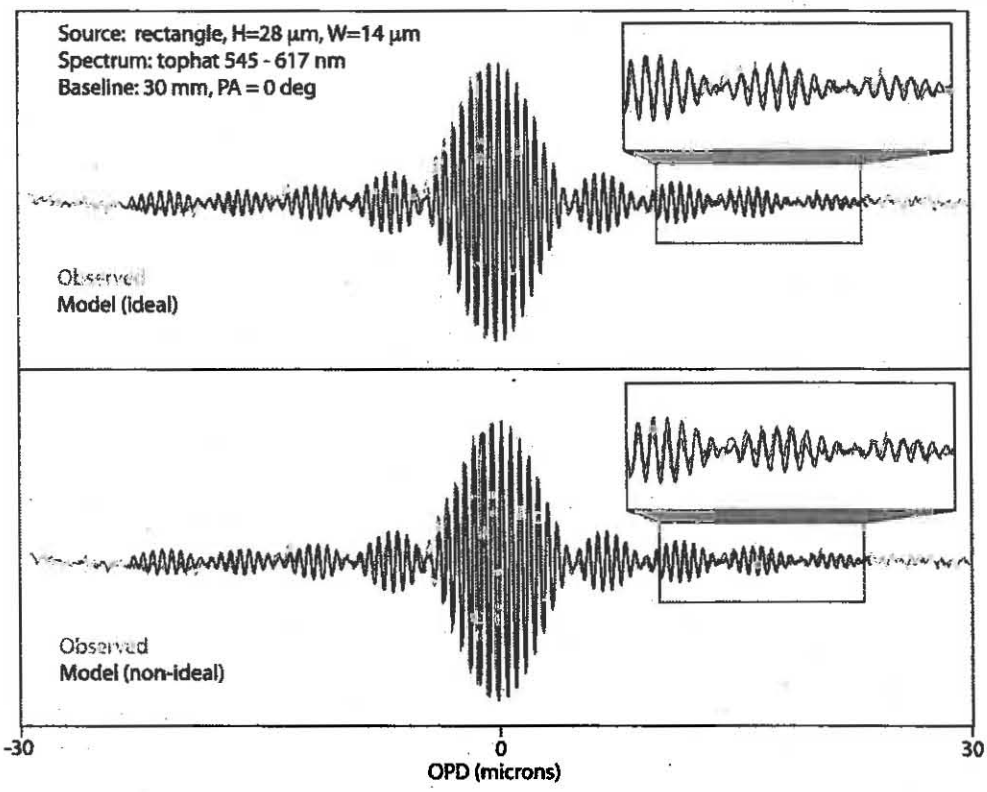

Figure 4. Model data from SsICOM show consistency with data from WIIT down to very fine details.

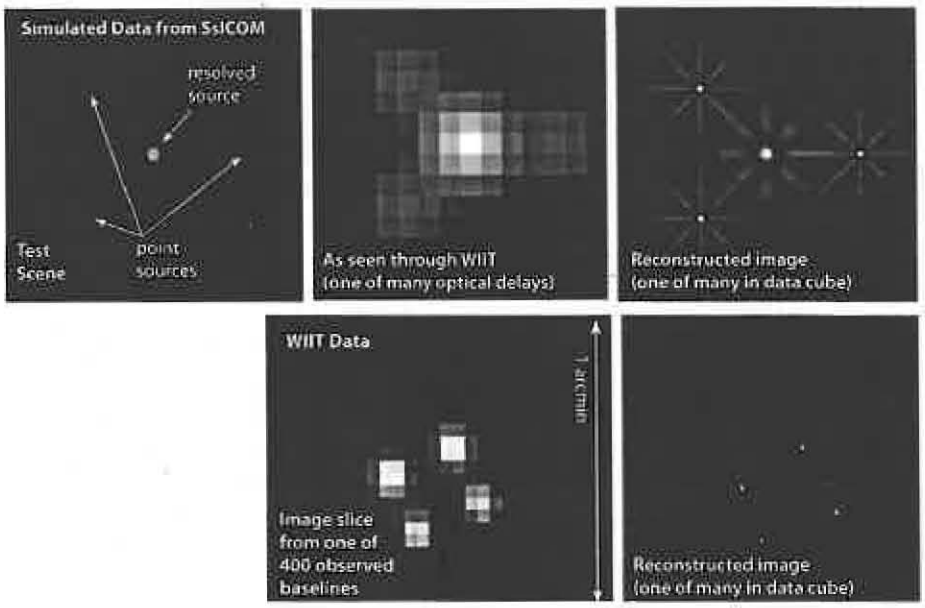

Figure 4. Spatio-Spectral Synthesis Software (S4) processing of synthetic data from SsICOM (top row) and WIIT (bottom row). Only 0, 45, 90, and 135 deg baseline angles were used in the top, accounting for the star-shaped "dirty beam." CLEAN deconvolution can be used to remove these artifacts, but they only appear when the u-v plane is sparsely sampled. Each synthesized image (right) is one of many drawn from the S4 output cube representing the test scene (top) or the scene that WIIT observed with many baselines (bottom).

Table 1a shows that imperfect reflecting surfaces and alignment are the dominant contributors to a net 16% loss of fringe visibility relative to a perfect interferometer. In other words, when an unresolved source (V = 1) is observed with WIIT, the measured visibility is about 0.84. We recently acquired the capability with CHIP to produce a source that is unresolved at the longest WIIT baselines. We now routinely embed three point sources in every observed scene to ensure accurate calibration.

Table 1a: Sources of Visibility Loss in WIIT

Source	Parameter ID	Parameter Value	Visibility Formula	Visibility Value
Alignment				
Coalignment at pupil	$1-\eta$	0.975	$1-\eta$	0.975
Tip/tilt at exit pupil	α	0.5"	$2J_1(\pi D\alpha/\lambda)/(\pi D\alpha/\lambda)$	0.995
Optics (RMS wavefront error)				
Collimating mirror	δ	15.75 nm	$\exp[-2\pi\delta/\lambda]^2$	0.97
Beamsplitter	δ	15 nm	$\exp[-2\pi\delta/\lambda]^2$	0.98
Interferometer mirrors	δ	10 nm	$\exp[-2N\pi\delta/\lambda]^2$	0.92
	N	9 mirrors		
Intensity Mismatch	ρ	92%	$2/(\rho^{1/2}+\rho^{-1/2})$	0.999
Positional Knowledge	δx	9.89 nm	$\mathrm{sinc}(2\pi\delta x/\lambda)$	0.999
Frame Exposure Time	t_{obs}	100 ms	$\mathrm{sinc}(2\pi v_{image} t_{obs}/\lambda)$	0.9995
Total Visibility Loss				0.84

Table 1b shows the fractional uncertainty in visibility attributable to potentially important noise sources. Photon counting is the dominant source of visibility uncertainty in WIIT. (In Table 1b, we assumed a relatively faint source, N_{cnts} = 5000.) Diagnostic data obtained in the AIM Lab demonstrated ~1 nm RMS wavefront stability in 30-s time intervals over a 10-m beam path, indicating that turbulence is a negligible contributor to visibility error. Thus, when operated in the AIM Lab, WIIT emulates a space-based far-IR interferometer with sensitive detectors. Calibrated WIIT visibility measurements are typically accurate to better than 2% (5% if the source visibility is 0.1 and it sits on a diffuse background of equal brightness per pixel).

Table 1b: Sources of Visibility Uncertainty in WIIT

Source	Parameter ID	Parameter Value	Visibility Uncertainty Formula	Visibility Uncertainty Value
Light Source				
Tip/tilt at exit pupil	$\delta I/I$	<0.5%	$\delta I/I$	<0.71%
Camera				
Bit Noise	σ_{bit}	0.5 counts	σ_{bit}/N_{cnts}	0.011%
Photon Counting	N_{elec}	2×10^5 e	$[(2/N_{elec})(2^{16}/N_{cnts})]^{1/2}$	1.40%
Camera noise (read noise, dark current)	σ_{det}	15 e	$(2\sigma_{det}/N_{elec})(2^{16}/N_{cnts})$	0.22%
Total Visibility Uncertainty				1.59%

5. FUTURE PLANS

Our goal is to mature wide-field spatio-spectral interferometry for future far-IR space mission applications to NASA's Technology Readiness Level (TRL) 6. To attain TRL 6, a technology must be demonstrated in a system model or prototype in an operational environment relevant to its intended space flight application. Here we are developing and proving a technique rather than a hardware technology, which is somewhat akin to proving the viability of the JWST wavefront sensing and control system. When used in the AIM Lab, WIIT is functionally and operationally equivalent to SPIRIT: its performance is limited by instrumental factors rather than environmental conditions. WIIT is our hardware system model. Our analytical optical system model SsICOM is used to verify a thorough understanding of the performance of the hardware system model, the effects of all relevant instrument parameters, and the wavelength and size scaling relationships applicable to each of those parameters. Our image construction software S4 is used to process

the interferometric data to obtain science quality data analogous to high-level pipeline data products from SPIRIT, i.e., calibrated hyperspectral image cubes. The ultimate acceptance test for wide-field spatio-spectral interferometry for space flight application is to demonstrate excellent agreement between synthesized hyperspectral cubes and observed, astronomically realistic "truth images" (see Figure 3), and a quantitative accounting for any differences in terms of understood instrumental effects. We plan to perform this test.

We will experiment with on-the-fly observing, the mode envisaged for SPIRIT. In the standard "step-and-scan" mode, the collector mirrors in WIIT are held stationary during an optical delay line scan, providing a discrete baseline sample and many temporal coherence measurements. This procedure is repeated for typically several hundred different baseline lengths and position angles. We will take advantage of CHIP's flexibility to implement an observing mode in which the baseline position angle is allowed to vary smoothly (by rotating the projected image) while the delay line is synchronously scanned, simulating the behavior of a rotating interferometer. We will test the effect of rotational smearing on the resulting constructed images with, and without, a deblurring algorithm that uses knowledge of the smooth motion to interpolate and regrid the interferometric data.

We will answer two practical questions: In realistic situations, how do factors such as photon noise, u-v plane undersampling, and motion smearing impact spatio-spectral interferometric data? And to what level do these factors need to be controlled to maintain the scientific capability of a far-IR spatio-spectral interferometer?

6. CONCLUSION

Wide-field spatio-spectral interferometry will open a new frontier in space astrophysics by enabling sensitive imaging and spectroscopic observations at far-infrared wavelengths with orders-of-magnitude better angular resolution than would be feasible otherwise. This will enable us to answer some of the most compelling questions in modern astrophysics, such as those posed in Section 1.

NASA sponsors this project through its Astrophysics Research and Analysis Program (NASA proposal number 06-APRA206-0162). We gratefully acknowledge student interns Mr. Daniel Liss, Ms. Melody Liu, and Mr. Elliot Teichman, who provided excellent assistance with the data analysis.

REFERENCES

[1] Leisawitz, D., et al. 2007, "The Space Infrared Interferometric Telescope (SPIRIT): High-resolution imaging and spectroscopy in the far-infrared," Adv. Sp. Res., 40, 689.

[2] Leisawitz, D., et al. 2009, "The Space Infrared Interferometric Telescope (SPIRIT): A Far-IR Observatory for High-resolution Imaging and Spectroscopy," white paper submitted to the Astronomy and Astrophysics Decadal Survey of 2010, http://astrophysics.gsfc.nasa.gov/cosmology/spirit/

[3] Helmich, F. and Ivison, R. 2009, "FIRI – a Far-InfraRed Interferometer for ESA," Experimental Astronomy, 23, 245.

[4] Harwit, M. et al. 2008, "A Kilometer-Baseline Far-Infrared/Submillimeter Interferometer in Space," in Progress in Astronautics & Aeronautics, vol. 224, ed. M.S. Allen (AIAA: Reston, VA), pp. 301 - 326 (SPECS "vision mission" study report)

[5] Rinehart, S.A. et al. 2010, "The Balloon Experimental Twin Telescope for infrared interferometry (BETTII)," in Optical and Infrared Interferometry II, eds. W.C. Danchi, F. Delplancke & J.K. Rajagopal, Proc. SPIE, 7734, 77340K.

[6] Rinehart, S.A. et al. 2012, "Design and status of the Balloon Experimental Twin Telescope for infrared interferometry (BETTII): an interferometer at the edge of space," in Optical and Infrared Interferometry III, eds. F. Delplancke, J.K. Rajagopal, & F. Malbet, Proc. SPIE, 8445 (this volume).

[7] Leisawitz, D.T. et al. 2003, "Wide-field imaging interferometry testbed I: purpose, testbed design, data, and synthesis algorithms," in Interferometry in Space, ed. Shao, M. Proc SPIE, 4852, 255.

[8] Rinehart, S.A. et al. 2003, "Wide-field imaging interferometry testbed II: implementation, performance, and plans," in Interferometry in Space, ed. Shao, M. Proc SPIE, 4852, 674.

[9] Leviton, D.B., et al. 2003, "Wide-field imaging interferometry testbed 3: metrology subsystem," in Interferometry in Space, ed. Shao, M., Proc. SPIE, 4852, 827.

[10] Rinehart, S.A. et al. 2004, "The wide-field imaging interferometry testbed: II. Characterization and calibration," in New Frontiers in Stellar Interferometry, ed. Traub, W. Proc. SPIE, 5491, 1790.
[11] Rinehart, S.A. et al. 2006, "The Wide-Field Imaging Interferometry Testbed: Recent Results," in Advances in Stellar Interferometry, eds. J.D. Monnier, M. Schöller, & W.C. Danchi, Proc. SPIE 6268, 626836.
[12] Thompson, A.K. et al. 2006, "Optical modeling of the wide-field imaging interferometry testbed," in Advances in Stellar Interferometry, eds. J.D. Monnier, M. Schöller, & W.C. Danchi, Proc. SPIE, 6268, 87.
[13] Rinehart, S.A. et al. 2007, "The Wide-Field Imaging Interferometry Testbed: Enabling Techniques for High Angular Resolution Astronomy," in UV/Optical/IR Space Telescopes: Innovative Technologies and Concepts III, eds. H.A. MacEwen & J.B. Breckinridge, Proc. SPIE, 66870F.
[14] Leisawitz, D., et al. 2007, "An Optical Model of the Wide-Field Imaging Interferometry Testbed," in UV/Optical/IR Space Telescopes: Innovative Technologies and Concepts III, eds. H.A. MacEwen & J.B. Breckinridge, Proc. SPIE, 66870J.
[15] Rinehart, S.A. et al. 2008, "The Wide-Field Imaging Interferometry Testbed (WIIT): Recent Progress and Results," in Optical and Infrared Interferometry, ed. M. Schöller, W.C. Danchi, & F. Delplancke, Proc. SPIE, 7013, 70132S.
[16] Lyon, R.G., et al. 2008, "Wide-Field Imaging Interferometry Testbed (WIIT): Image Construction Algorithms," in Optical and Infrared Interferometry, ed. M. Schöller, W.C. Danchi, & F. Delplancke, Proc. SPIE, 7013, 70131M.
[17] Rinehart, S.A. et al. 2010, "Recent Progress in Wide-Field Imaging Interferometry," Optical and Infrared Interferometry II, edited by William C. Danchi, Françoise Delplancke, Jayadev K. Rajagopal, Proc. SPIE, 7734, 77342D.
[18] Bolcar, M.R., Leisawitz, D.T., Maher, S.F., and Rinehart, S.A. 2012, "Demonstration of the wide-field imaging interferometer testbed using a calibrated hyperspectral image projector," in Optical and Infrared Interferometry III, eds. F. Delplancke, J.K. Rajagopal & F. Malbet, Proc. SPIE, Paper 8445 (this volume).
[19] Lyon, R.G. et al. 2012, "Wide-field imaging interferometry spatial-spectral image synthesis algorithms," in Optical and Infrared Interferometry III, eds. F. Delplancke, J.K. Rajagopal & F. Malbet, Proc. SPIE 8445 (this volume).
[20] Contos, A.R. et al. 2008, "Verification of the James Webb Space Telescope (JWST) wavefront sensing and control system," in Optical, Infrared, and Millimeter, eds. J.M. Oschmann, Jr., M.W.M. de Graauw & H.A. MacEwen, Proc. of SPIE, 7010, 70100S.
[21] Michelson, A.A., Morley, E.W. 1887, ""On the Relative Motion of the Earth and the Luminiferous Ether." Amer. J. Sci. 34, 333.
[22] Michelson, A.A., and Pease, F.G. 1921, "Measurement of the diameter of alpha Orionis with the interferometer," ApJ, 53, 249.
[23] Born M., and Wolfe, E. 1999, Principles of Optics, 5th edition, Pergamon, Oxford.
[24] Mariotti, J.-M., and Ridgway, S.T. 1988, "Double Fourier spatio-spectral interferometry - Combining high spectral and high spatial resolution in the near infrared," A&A, 195, 350.
[25] Cornwell, T. J. 1988, "Radio-interferometric imaging of very large objects," A&A, 202, 316.
[26] Bhatnagar, S., Golap, K., and Cornwell, T. J. 2005, "Mosaicing with interferometers: An Efficient Algorithm for Imaging and Image Plane Corrections," in Astronomical Data Analysis Software and Systems XIV, eds. Shopbell, P., Britton, M. & Ebert R., ASP Conference Series, 347, 96.
[27] Rice, J.P., Brown, S.W., Johnson, B.C., and Neira, J.E. 2006, "Hyperspectral image projectors for radiometric applications," Metrologia 43, S61-S65.
[28] Rice, J.P., Brown, S.W., and Neira, J.E. 2006, "Development of hyperspectral image projectors," in Infrared Spaceborne Remote Sensing XIV, ed. M. Strojnik, Proc. SPIE, 6297, 629701.
[29] Prasad, S. and Kulkarni, S.R. 1989, "Noise in optical synthesis images. I. Ideal Michelson interferometer," J. Opt. Soc. Am. A, 6, 1702.
[30] Zmuidzinas, J. 2003, "Cramer–Rao sensitivity limits for astronomical instruments: implications for interferometer design," J. Opt. Soc. Am. A, 20, 218.